J|A|C|S ARTICLES

Published on Web 04/19/2010

Transition State Analogue Structures of Human Phosphoglycerate Kinase Establish the Importance of Charge Balance in Catalysis

Matthew J. Cliff,[†] Matthew W. Bowler,*[,‡] Andrea Varga,[§] James P. Marston,[†] Judit Szabó,[§] Andrea M. Hounslow,[†] Nicola J. Baxter,[†,⊥] G. Michael Blackburn,[†] Mária Vas,[§] and Jonathan P. Waltho*[,†,⊥]

The Krebs Institute & The Department of Molecular Biology and Biotechnology, The University of Sheffield, Firth Court, Western Bank, Sheffield S10 2TN, U.K., Structural Biology Group, European Synchrotron Radiation Facility, 6 rue Jules Horowitz, F-38043 Grenoble, France, Institute of Enzymology, Biological Research Center, Hungarian Academy of Sciences, P.O. Box 7, H-1518 Budapest, Hungary, Manchester Interdisciplinary Biocentre, University of Manchester, Manchester M1 7DN, U.K.

Received February 9, 2010; E-mail: j.waltho@shef.ac.uk; bowler@esrf.fr

Abstract: Transition state analogue (TSA) complexes formed by phosphoglycerate kinase (PGK) have been used to test the hypothesis that balancing of charge within the transition state dominates enzyme-catalyzed phosphoryl transfer. High-resolution structures of trifluoromagnesate (MgF_3^-) and tetrafluoroaluminate (AlF_4^-) complexes of PGK have been determined using X-ray crystallography and ^{19}F-based NMR methods, revealing the nature of the catalytically relevant state of this archetypal metabolic kinase. Importantly, the side chain of K219, which coordinates the α-phosphate group in previous ground state structures, is sequestered into coordinating the metal fluoride, thereby creating a charge environment complementary to the transferring phosphoryl group. In line with the dominance of charge balance in transition state organization, the substitution K219A induces a corresponding reduction in charge in the bound aluminum fluoride species, which changes to a trifluoroaluminate (AlF_3^0) complex. The AlF_3^0 moiety retains the octahedral geometry observed within AlF_4^- TSA complexes, which endorses the proposal that some of the widely reported trigonal AlF_3^0 complexes of phosphoryl transfer enzymes may have been misassigned and in reality contain MgF_3^-.

Introduction

Phosphoglycerate kinase (PGK, EC 2.7.2.3) catalyzes the transfer of phosphate from 1,3-bisphosphoglycerate (BPG) to ADP in the first ATP-generating step of glycolysis. As a major controller of flux, PGK is an important target for the disruption of glycolysis in anaerobic pathogens such as *Trypanosoma* and *Plasmodium* species[1] that depend solely on this pathway for energy metabolism. In mammals, PGK has more widespread roles, particularly in oncogenesis and development. Elevated PGK concentrations inhibit plasmin-mediated angiogenesis in response to hypoxia, required for solid tumor development. Intracellular PGK inhibits the expression of plasmin activating factors like uPAR,[2] and extracellular PGK promotes plasmin autolysis, producing Angiostatin.[3] Consequently, carcinoma cells transfected to overexpress PGK have severely limited growth and invasive ability.[4] PGK expression also affects DNA replication and repair in mammalian cells.[5] Furthermore, it promotes the activity of L-nucleoside analogue drugs, including cancer treatments[6] and anti-retrovirals, which are specifically activated *in vivo* through phosphorylation by PGK.[7,8] Modulation of these PGK activities using knowledge-based approaches would benefit greatly from a thorough understanding of its catalytic mechanism.

In a wider context, PGK is an archetype of phosphoryl group transfer enzymes. The manipulation and stabilities of phosphate mono- and diesters underpin the entire biosphere, being involved in processes ranging from the storage and manifestation of genetic information to energy generation, signaling, and differentiation.[9] As structural components, they show remarkable resistance to spontaneous hydrolysis under near physiological

[†] University of Sheffield.
[‡] European Synchrotron Radiation Facility.
[§] Institute of Enzymology.
[⊥] University of Manchester.

(1) Opperdoes, F. R. *Annu. Rev. Microbiol.* **1987**, *41*, 127–131.
(2) Shetty, S.; Ganachari, M.; Liu, M.-C.; Azghani, A.; Muniyappa, H.; Idell, S. *Am. J. Physiol. Lung Cell Mol. Physiol.* **2005**, *289*, L591–L598.
(3) Lay, A. J.; Jiang, X.-M.; Kisker, O.; Flynn, E.; Underwood, A.; Condron, R.; Hogg, P. J. *Nature* **2000**, *408*, 869–873.
(4) Tang, S.-J.; Ho, M.-Y.; Cho, H.-C.; Lin, Y.-C.; Sun, G. H.; Chi, K.-H.; Wang, Y.-S.; Jhou, R.-S.; Yang, W.; Sun, K.-H. *Int. J. Cancer* **2008**, *123*, 2840–2848.
(5) Poponda, O.; Fox, G.; Thielkmann, H. W. *Biochim. Biophys. Acta* **1998**, *1397*, 102–117.
(6) Lam, W.; Bussom, S.; Cheng, Y.-C. *Mol. Cancer Ther.* **2009**, *8*, 415–423.
(7) Krishnan, P.; Gullen, E. A.; Lam, W.; Dutschman, G. E.; Grill, S. P.; Cheng, Y.-C. *J. Biol. Chem.* **2003**, *278*, 36726–36732.
(8) Mathe, C.; Gosselin, G. *Antiviral Res.* **2006**, *71*, 276–281.
(9) Cleland, W. W.; Hengge, A. C. *Chem. Rev.* **2006**, *106*, 3252–3278.

 © 2010 American Chemical Society

conditions, yet enzyme-catalyzed phosphoryl group transfer reactions have sufficiently high turnover numbers to support a vast array of biological processes. Indeed, the transfer of phosphate monoesters is associated with the largest enzymatic rate enhancements yet identified,[10] with accelerations (k_{cat}/k_{uncat}) in the range of 10^{21}. The reaction is widely accepted to proceed through a trigonal, planar phosphoryl species, PO_3^-, but most details of its nature and its interactions with enzymes remain ill-defined.[9,11] This places limitations on computational approaches to deciphering the source of the remarkable catalytic proficiency of phosphoryl transfer enzymes.

A substantial step forward in understanding the fundamental mechanism of phosphoryl group transfer by enzymes came through the use of aluminum and magnesium fluoride species[12,13] and transition metal oxoanions[14] as transition state analogues (TSAs) of the planar PO_3^- group. The metal fluoride TSA complexes are particularly informative because ^{19}F NMR can be used to validate the interpretation of X-ray diffraction data and to report on the local electrostatic and protonic environments in the vicinity of the transferring phosphoryl group.[13,15−17] Recent work has demonstrated that trigonal bipyramidal (TBP) trifluoromagnesate (MgF_3^-) complexes readily assemble in the active site of a range of phosphoryl transfer enzymes,[13,15,18,19] where the MgF_3^- is axially coordinated by donor and acceptor oxygen atoms. MgF_3^- is isoelectronic and close to isosteric with the transferring PO_3^- group. In the presence of Al^{3+}, MgF_3^- was shown in a number of enzymes to be readily out-competed by tetrafluoroaluminate (AlF_4^-),[15] which, although having the same net charge as PO_3^-, has non-isosteric octahedral geometry. This indicates that these enzymes are prioritizing retention of charge rather than geometry in their selection of a surrogate for PO_3^-. Moreover, the accommodation of a singly, negatively charged moiety, such as MgF_3^- or AlF_4^-, ensures that the number of positively and negatively charged groups contributing to the active site is exactly balanced.[15] A dominant role for such charge balance in transition state (and TSA) stabilization by phosphoryl transfer enzymes (the charge-balance hypothesis) was suggested[20] on the basis of observations on the binding of bisubstrate analogues to yeast PGK (ScPGK). This hypothesis rationalizes, for example, inhibitor studies on nucleotide kinases,[21,22] where isosteric analogues bound significantly less well than similar molecules that were non-isosteric, yet had a net charge more closely resembling the putative transition state. In contrast, over 30 phosphoryl transfer enzymes have been reported to contain TBP trifluoroaluminate (AlF_3^0) species in the active sites, acting as TSAs that are near-isosteric but not isoelectronic with PO_3^-. Such assignments imply that these enzymes prioritize retention of geometry rather than the charge of the surrogate for PO_3^- to such a degree that the Al^{3+} ion relinquishes its preferred octahedral coordination[23] (the antithesis of the charge-balance hypothesis). However, AlF_3^0 has not hitherto been identified unambiguously in an enzyme TSA complex in solution, leading to the proposal[15] that the metal fluoride moieties in these crystals may have been misidentified and are in reality MgF_3^-.

In order to test the charge-balance hypothesis in an archetypal phosphoryl transfer enzyme and to provide the first experimental insights into TS organization in PGK, we have prepared and analyzed metal fluoride complexes of the PGK1 isoform of human PGK (HsPGK). While there is a wealth of structural and biophysical data that give a general picture of the mode of action of PGK,[24] there are inconsistencies relating to the nature of the species responsible for phosphoryl group transfer.[25−27] PGK comprises two similarly sized Rossmann fold domains—the N-domain binds BPG or 3-phosphoglycerate (3PG), while the C-domain binds the nucleotides. Structures have been determined, showing the domains in an open conformation (e.g., in pig PGK (SsPGK-ATP complex)[28]) and in a more closed conformation (*Trypanosoma brucei* PGK (TbPGK-3PG-ADP complex)[26] and *Thermotoga maritima* PGK (TmPGK-3PG-AMPPNP complex)[27]), which allows the substrates to come into contact. Such domain closure has been demonstrated in solution for HsPGK in the presence of 3PG and ATP.[29] Here we report the first structures of the catalytically relevant, fully closed conformation for any PGK, which resolve ambiguities associated with previous interpretations of the mechanism of phosphoryl transfer. The structures accurately identify the role of the catalytic Mg^{2+}, reveal a novel mechanism for countering the anionic charge on the transferring PO_3^- group by an enzyme, and provide a test of the charge-balance hypothesis in the control of enzyme-catalyzed phosphoryl transfer. As predicted by this hypothesis, the removal of a key positive charge in the enzyme by mutation directly induces a corresponding reduction in charge by the aluminum fluoride moiety in the TSA complex.

Results and Discussion

HsPGK-3PG-MgF_3^--ADP TSA Complex. *Geobacillus stearothermophilus* PGK (GsPGK) was previously shown using ^{19}F NMR spectroscopy to populate a GsPGK-3PG-AlF_4^--ADP TSA complex, but an equivalent MgF_3^- complex was too poorly populated to be detected.[15] Population of MgF_3^- TSA complexes

(10) Lad, C.; Williams, N. H.; Wolfenden, R. *Proc. Natl. Acad. Sci. U.S.A.* **2003**, *100*, 5607–5610.
(11) Rosta, E.; Kamerlin, S. C. L.; Warshel, A. *Biochemistry* **2008**, *47*, 3725–3735.
(12) Wittinghofer, A. *Curr. Biol.* **1997**, *7*, R682–R685.
(13) Baxter, N. J.; Olguin, L. F.; Golicnik, M.; Feng, G.; Hounslow, A. M.; Bermel, W.; Blackburn, G. M.; Hollfelder, F.; Waltho, J. P.; Williams, N. H. *Proc. Natl. Acad. Sci. U.S.A.* **2006**, *103*, 14732–14737.
(14) Messmore, J. M.; Raines, R. T. *J. Am. Chem. Soc.* **2000**, *122*, 9911–9916.
(15) Baxter, N. J.; Blackburn, G. M.; Marston, J. M.; Hounslow, A. M.; Cliff, M. J.; Bermel, W.; Williams, N. H.; Hollfelder, F.; Wemmer, D. E.; Waltho, J. P. *J. Am. Chem. Soc.* **2008**, *130*, 3952–3958.
(16) Baxter, N. J.; Hounslow, A. M.; Bowler, M. W.; Williams, N. H.; Blackburn, G. M.; Waltho, J. P. *J. Am. Chem. Soc.* **2009**, *131*, 16334–16335.
(17) Baxter, N. J.; Bowler, M. W.; Alizadeh, T.; Cliff, M. J.; Hounslow, A. M.; Wu, B.; Berkowitz, D. B.; Williams, N. H.; Blackburn, G. M.; Waltho, J. P. *Proc. Natl. Acad. Sci. U.S.A.* **2010**, *107*, 4555–4560.
(18) Graham, D. L.; Lowe, P. N.; Grime, G. W.; Marsh, M.; Rittinger, K.; Smerdon, S. J.; Gamblin, S. J.; Eccleston, J. F. *Chem. Biol.* **2002**, *9*, 375–381.
(19) Lee, J. Y.; Yang, W. *Cell* **2006**, *127*, 1349–1360.
(20) Williams, D. M.; Jakeman, D. L.; Vyle, J. S.; Williamson, M. P.; Blackburn, G. M. *Bioorg. Med. Chem. Lett.* **1998**, *8*, 2603–2608.
(21) Lienhard, G. E.; Secemski, I. L. *J. Biol. Chem.* **1973**, *248*, 1121–1123.
(22) Wiesmüller, L.; Scheffzek, K.; Kliche, W.; Goody, R. S.; Wittinghofer, A.; Reinstein, J. *FEBS Lett.* **1995**, *363*, 22–24.
(23) Pinkas, J.; Roesky, H. W. *J. Fluorine Chem.* **2003**, *122*, 125–150.
(24) Vas, M.; Varga, A.; Gráczer, E. *Curr. Protein Pept. Sci.* **2010**, *11*, 118–147.
(25) Szabó, J.; Varga, A.; Flachner, B.; Konarev, P. V.; Svergun, D. I.; Závodszky, P.; Vas, M. *Biochemistry* **2008**, *47*, 6735–6744.
(26) Bernstein, B. E.; Michels, P. A. M.; Hol, W. G. J. *Nature* **1997**, *385*, 275–278.
(27) Auerbach, G.; Huber, R.; Grattinger, M.; Zaiss, K.; Schurig, H.; Jaenicke, R.; Uwe, J. *Structure* **1997**, *5*, 1475–1483.
(28) Flachner, B.; Kovári, Z.; Varga, A.; Gugolya, A.; Vonderviszt, F.; Náray-Szabó, G.; Vas, M. *Biochemistry* **2004**, *43*, 3436–3449.
(29) Varga, A.; Flachner, B.; Konarev, P.; Gráczer, E.; Szabó, J.; Svergun, D.; Závodszky, P.; Vas, M. *FEBS Lett.* **2006**, *580*, 2698–2706.

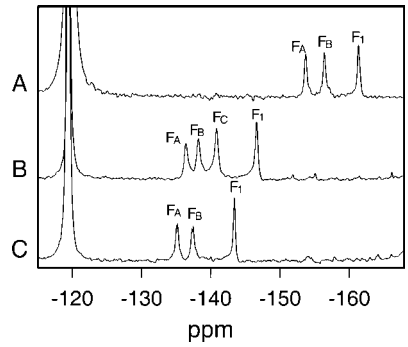

Figure 1. ^{19}F NMR spectra of HsPGK TSA complexes (A) HsPGK-3PG-MgF_3^--ADP TSA complex ($F_A = -153$, $F_B = -156$, $F_1 = -161$ ppm). The most upfield ^{19}F resonance is assigned as F_1 (see Figure 3A,B). The assignment of the other ^{19}F resonances is ambiguous, and therefore, the resonances are labeled alphabetically from left to right on the basis of chemical shift. Free F^- resonates at −119 ppm. (B) HsPGK-3PG-AlF_4^--ADP TSA complex ($F_A = -136$, $F_B = -138$, $F_C = -141$, $F_1 = -146$ ppm). Again, the most upfield ^{19}F resonance is assigned as F_1 (see Figure 5). The other resonances are labeled alphabetically from left to right on the basis of chemical shift and do not necessarily indicate equivalence of nuclei between the spectra. (C) HsPGK(K219A)-3PG-AlF_3^0-ADP TSA complex ($F_A = -135$, $F_B = -137$, $F_1 = -143$ ppm). The similarly narrow line widths compared to (B) for the ^{19}F resonances indicate that the loss of a fluorine resonance on switching from HsPGK to HsPGK(K219A) is inconsistent with selective exchange broadening effects.

is counteracted by the inherent instability of MgF_3^- in solution.[13] However, the MgF_3^- TSA complex of HsPGK (HsPGK-3PG-MgF_3^--ADP TSA complex) is readily detectable (Figure 1A and Table S1, Supporting Information). The value of k_{cat} for HsPGK is >10-fold faster than that for GsPGK,[30,31] and the greater affinity for MgF_3^- points to this increase in rate constant being the result of greater stabilization of the TS in the human enzyme. The resolution and relaxation properties of the three ^{19}F resonances of the MgF_3^- moiety indicate that the protein-bound fluorine nuclei are held in distinct sites, with no significant intersite exchange on the chemical shift time scale ($t_{0.5} > 10^{-3}$ s). ^{1}H NMR chemical shift changes within HsPGK (Figure S1A, Supporting Information) are consistent with TSA complex formation being associated with domain closure.

The HsPGK-3PG-MgF_3^--ADP TSA complex crystallized in the orthorhombic space group $P2_12_12_1$ with one molecule in the asymmetric unit, with novel unit cell dimensions for crystals of PGK. The structure was solved using molecular replacement to a resolution of 1.47 Å (see Experimental Procedures and Table 1), revealing a closed conformation (Figure 2A). The electron density maps were of excellent quality for residues 3−132 and 143−417, and the ligands were clearly located in the active site (Figure 2B), with a MgF_3^- moiety occupying the position of the transferring PO_3^- group. The MgF_3^- has TBP geometry with the equatorial positions occupied by the three fluorine atoms and the two axial positions occupied by donor and acceptor oxygen atoms from ADP and 3PG. Figure 3A,B details the coordination of the three equatorial fluorine atoms. The ^{19}F resonance at −161 ppm (Figure 1A) can be assigned as corresponding to F_1, owing to its small deuterium sum isotope shift[16,17] and relatively narrow line width (Table S1, Supporting Information), but the environments of F_2 and F_3 are too similar to permit an assignment of resonances F_A and F_B. Notably, the coordinating hydrogen bonds have heavy atom separations in the range of 2.70−2.96 Å, with no evidence for short strong hydrogen bonds.[32,33]

The catalytically relevant coordination of the essential Mg^{2+} is resolved by the structure of the HsPGK-3PG-MgF_3^--ADP TSA complex. It is octahedrally coordinated by the pro*R* oxygen atoms of both the α- and β-phosphates of ADP as well as the metal fluoride that mimics the transferring γ-phosphoryl group (Figure 3A,B). The remaining ligands comprise D374:Oδ and two water molecules. It is the first example of an anticlockwise facial coordination of the catalytic Mg^{2+} in any nucleotide phosphoryl transfer enzyme (Figure S2, Supporting Information). Such coordination in the TSA indicates a distinct role for γ-phosphate coordination by Mg^{2+} during catalysis and, for example, explains the response of PGK to chiral thiophosphate analogues of ATP.[34] The specificity of PGK for the α-S_p and β-S_p diastereoisomers of these analogues (where the sulfur atom replaces the pro*S* oxygen) is because sulfur cannot readily coordinate the catalytic Mg^{2+} and therefore the α-R_p and β-R_p diastereoisomers cannot bind to the enzyme.

Domain closure upon TSA complex formation occurs without substantial changes in the topology of PGK (Figure 2A). It retains the canonical 15 α-helices and 15 β-strands, arranged in two α/β Rossmann folds, with a three-strand β-sheet insertion in the C-domain and additional α-helices in both domains (helix-4 in the N-domain and helix-9 in the C-domain). Helix-7 links the two domains. However, in the HsPGK-3PG-MgF_3^--ADP TSA complex, the domains are rotated 33.5° toward each other from their positions in the SsPGK-ATP complex[28] and a further 5.5° from their positions in the structure previously thought to be fully closed (TbPGK-3PG-ADP) (Figure 4A,B).[35] Domain closure occurs primarily through alterations in the backbone dihedral angles in two previously identified hinges, one at the C-terminus of helix-7 and one at the C-terminus of β-strand L[26,36] (Table S2, Supporting Information), which reduces the distance between donor and acceptor oxygen atoms to 4.3 Å (compared to 5.0 Å in the TbPGK-3PG-ADP complex). Closure is also associated with the formation of three salt bridges—two (R65-D218 and K29-E293; HsPGK numbering) identified previously in the TbPGK-3PG-ADP complex and R170-D218. Intriguingly, domain closure does not fully exclude water from the mimic of the transferring PO_3^- group. Four active site water molecules are resolved in the HsPGK-3PG-MgF_3^--ADP TSA complex, two of which coordinate the catalytic magnesium and one which contacts the MgF_3^- moiety. Only the fourth water molecule is sequestered from bulk solvent, suggesting that desolvation is not an essential feature of catalysis by PGK.

In addition to revealing the full extent of domain closure, the HsPGK-3PG-MgF_3^--ADP TSA structure accurately identifies the role in phosphoryl transfer for a key basic side chain of PGK, namely, K219. Site-directed mutagenesis studies have already identified R38[31,37] and K215[31,38] as essential compo-

(30) Parker, M. J.; Sessions, R. B.; Badcoe, I. G.; Clarke, A. R. *Folding Des.* **1996**, *1*, 145–156.
(31) Flachner, B.; Varga, A.; Szabó, J.; Barna, L.; , I.; Gyimesi, G.; Závodszky, P.; Vas, M. *Biochemistry* **2005**, *44*, 16853–16865.
(32) Gerlt, J. A.; Kreevoy, M. M.; Cleland, W. W.; Frey, P. A. *Chem. Biol.* **1997**, *4*, 259–267.
(33) Harris, T. K.; Mildvan, A. S. *Proteins* **1999**, *35*, 275–282.
(34) Jaffe, E. K.; Nick, J.; Cohn, M. *J. Biol. Chem.* **1982**, *257*, 7650–7656.
(35) Hayward, S.; Lee, R. A. *J. Mol. Graphics Modell.* **2002**, *21*, 181–183.
(36) Szilágyi, A. N.; Ghosh, M.; Garman, E.; Vas, M. *J. Mol. Biol.* **2001**, *306*, 499–511.
(37) Sherman, M. A.; Szpikowska, B. K.; Dean, S. A.; Mathiowetz, A. M.; McQueen, N. L.; Mas, M. T. *J. Biol. Chem.* **1990**, *265*, 10659–10665.
(38) Varga, A.; Lionne, C.; Lallemand, P.; Szabó, J.; Adamek, N.; Valentin, C.; Vas, M.; Barman, T.; Chaloin, L. *Biochemistry* **2009**, *48*, 6998–7008.

Table 1. Data Processing and Refinement Statistics

structure	HsPGK-3PG-MgF_3^--ADP	HsPGK-3PG-AlF_4^--ADP	HsPGK(K219A)-3PG-AlF_3^0-ADP
space group	$P2_12_12_1$	$P2_12_12_1$	$P2_12_12_1$
wavelength (Å)	0.933	0.933	0.933
unit cell dimensions (Å) *a, b, c*	39.4, 92.2, 109.0	39.2, 92.0, 108.1	39.4, 91.6, 108.5
resolution range (Å)	20−1.47	20−1.50	20−1.56
number of unique reflections	68247	61523	55495
multiplicity[a]	3.6 (3.5)	2.8 (2.7)	2.7 (2.6)
completeness[a] (%)	99.1 (98.0)	97.4 (96.2)	98.0 (95.9)
R_{merge}[a,b]	0.05 (0.32)	0.06 (0.30)	0.06 (0.28)
$\langle I/\sigma(I)\rangle$[a]	13.3 (3.3)	11.4 (3.0)	10.9 (3.7)
Wilson B factor (Å^2)	14	15	15
water molecules	617	468	465
R factor[c] (%)	16.1	16.4	16.6
free *R* factor[d] (%)	18.6	19.8	20.2
rms deviations:			
bonds (Å)	0.01	0.01	0.02
angles (°)	1.8	1.6	1.2

[a] Statistics for the highest resolution bin (1.55−1.47 Å: HsPGK-3PG-MgF_3^--ADP; 1.58−1.50 Å: HsPGK-3PG-AlF_4^--ADP; 1.64−1.56 Å: HsPGK(K219A)-3PG-AlF_3^0-ADP) are shown in parentheses. [b] $R_{merge} = \Sigma_h\Sigma_i|I(h) - I(h)_i|/\Sigma_h\Sigma_i I(h)_i$, where $I(h)$ is the mean weighted intensity after rejection of outliers. [c] $R = \Sigma_{hkl}||F_{obs}| - k|F_{calc}||/\Sigma_{hkl}|F_{obs}|$, where F_{obs} and F_{calc} are the observed and calculated structure factor amplitudes. [d] $R_{free} = \Sigma_{hkl\subset T}||F_{obs}| - k|F_{calc}||/\Sigma_{hkl\subset T}|F_{obs}|$, where T is the test set of data omitted from refinement (5% in this case).

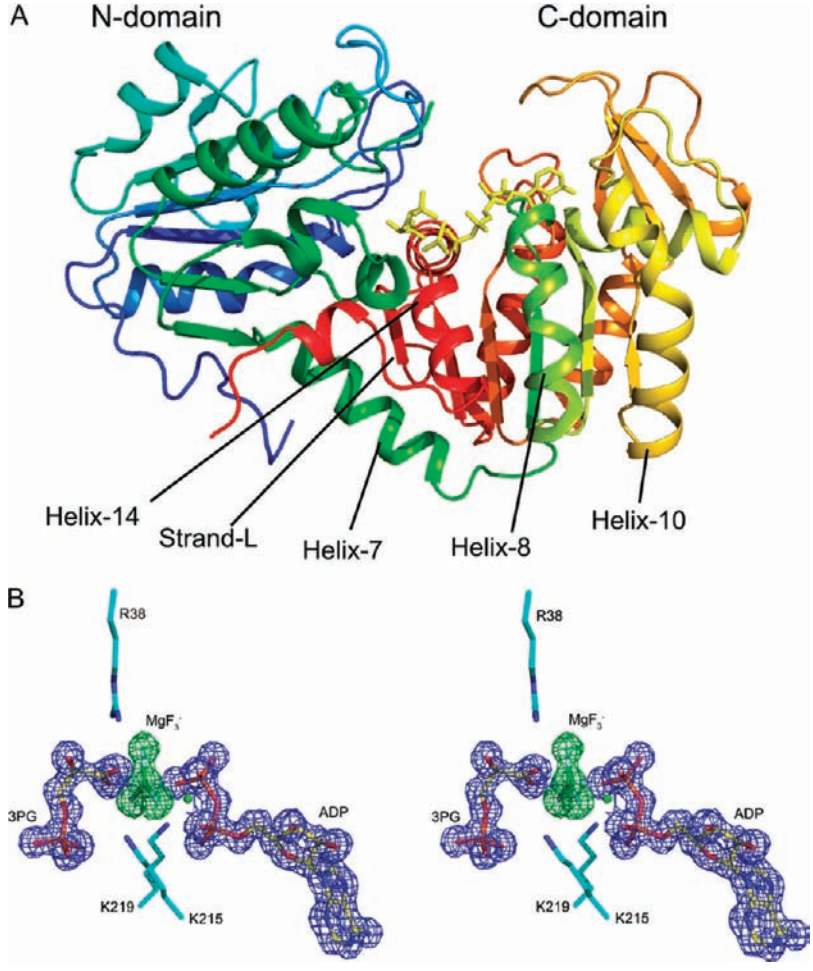

Figure 2. Structure of the fully closed HsPGK-3PG-MgF_3^--ADP TSA complex. (A) Crystal structure of the HsPGK-3PG-MgF_3^--ADP TSA complex shown as a cartoon, colored blue to red from N- to C-terminus. The TSA ligands are shown as sticks, the secondary structure elements discussed in the text are labeled. (B) Electron density (1.47 Å resolution) in the active site of the HsPGK-3PG-MgF_3^--ADP TSA complex shown in stereo. The difference electron density (F_o-F_c) for MgF_3^- before its inclusion in the model is shown as a green mesh contoured at 3σ. The $2F_o-F_c$ electron densities for the 3PG and ADP ligands are shown as a blue mesh contoured at 1.5σ. The coordinating lysine and arginine side chains (cyan) and the catalytic Mg^{2+} (green sphere) are also indicated.

nents of the catalytic machinery, both of which coordinate fluorine atoms in the HsPGK-3PG-MgF_3^--ADP TSA complex. An important role for K219 was also inferred from mutagenesis,[25] but in all previous PGK structures, this residue has a common position too distant from the putative position of the transferring PO_3^- group to interact with it (Figure 3C). Uniquely,

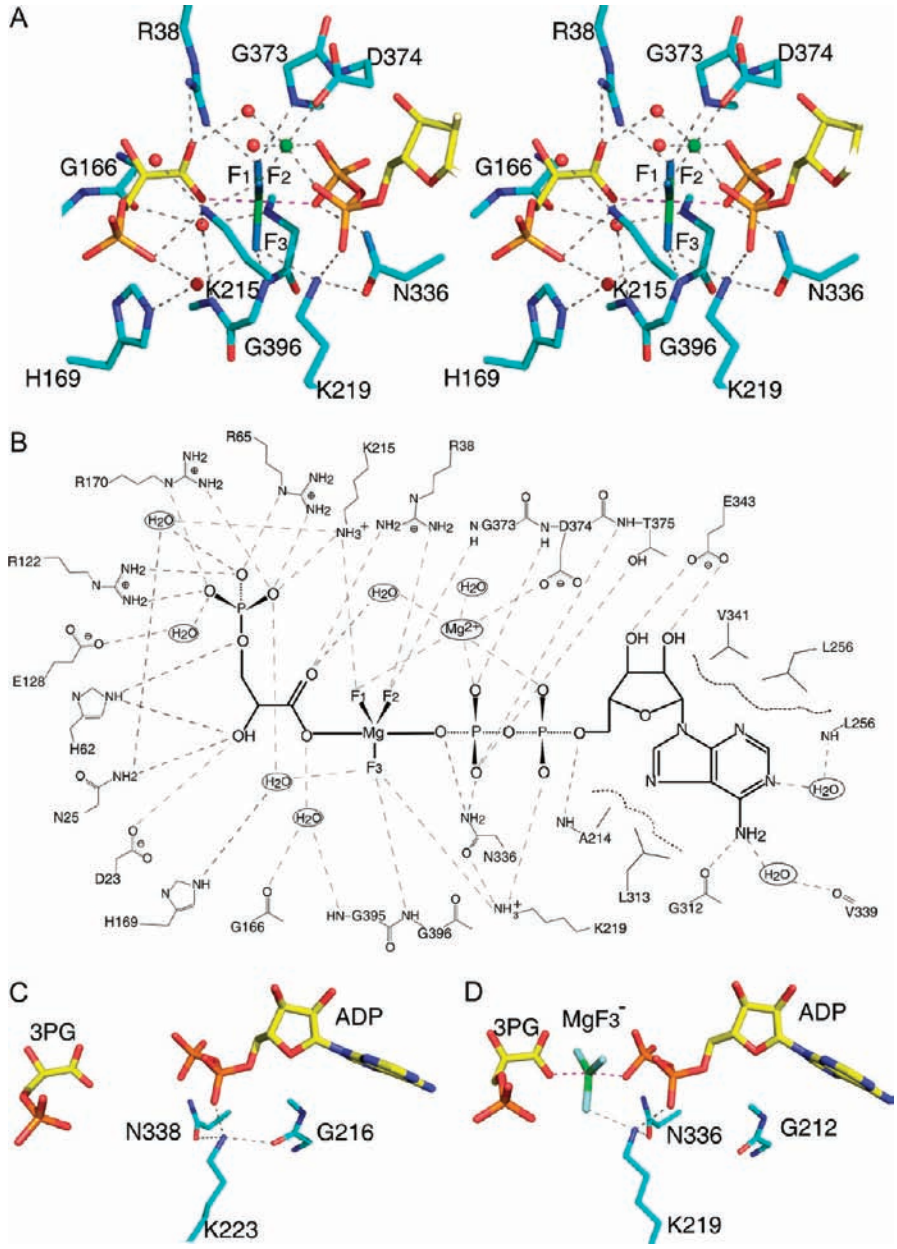

Figure 3. Structure of the HsPGK-3PG-MgF_3^--ADP TSA complex active site. (A) Stereo view of the MgF_3^- moiety (pale blue and green) showing the protein coordination to the equatorial fluorine atoms and the axial coordination by the 3PG and ADP ligands (yellow). Gray dashes and purple dashes indicate hydrogen bonds and the axial Mg−O bonds, respectively. Four water molecules (red spheres) are resolved in the active site, two of which coordinate the catalytic Mg^{2+} (green sphere). (B) Schematic representation of the network of hydrogen bonding interactions (<2.9 Å) in the active site. (C) In the TbPGK-3PG-ADP complex, the ε-amino group of K223 (K219 in HsPGK) is hydrogen bonded to G216 carbonyl oxygen (G212 in HsPGK), the proS α-oxygen of ADP, and the γ-amide group of N338 (N336 in HsPGK). (D) In the fully closed HsPGK-3PG-MgF_3^--ADP TSA complex, the K219 side chain is rotated 24° around the axis of helix-8 from its location in the TbPGK-3PG-ADP complex, which places the ε-amino group within hydrogen bonding distance of the MgF_3^- moiety.

in the HsPGK-3PG-MgF_3^--ADP TSA complex, the K219 side chain is rotated around the axis of helix-8 so that the ε-amino group hydrogen bonds with F_3 of the MgF_3^- moiety (Figure 3D). K219 has previously been highlighted as a critical residue in the hydrogen bonding networks that alter upon domain closure, through its interaction with N336:Oδ.[29] Thus, the movement of K219:Nζ induced by the negative charge at the transferring phosphate position is likely to be transmitted throughout the interdomain region, triggering and/or stabilizing the closure mechanism.

The high resolution of the HsPGK-3PG-MgF_3^--ADP TSA structure also resolves the source of conformational change in helix-8 upon domain reorientation. In the open structures, helix-8 bends away from the N-domain because the first turn of the helix is disrupted by water molecules that bridge two regular hydrogen bonds (Figure 4C). One of the waters is hydrogen bonded to the γ-carboxylate group of E403 at the C-terminus of helix-14. Upon closure, the relative positions of helix-14 and helix-8 change such that the E403 γ-carboxylate group is now located by the second turn of helix-8 (Figure 4D). The two water molecules disrupting the first turn of the helix are ejected, and two water molecules are introduced into the second turn of helix-8, again coordinated by E403. Consequently, helix-8 now bends toward the N-domain and the interdomain region, allowing the

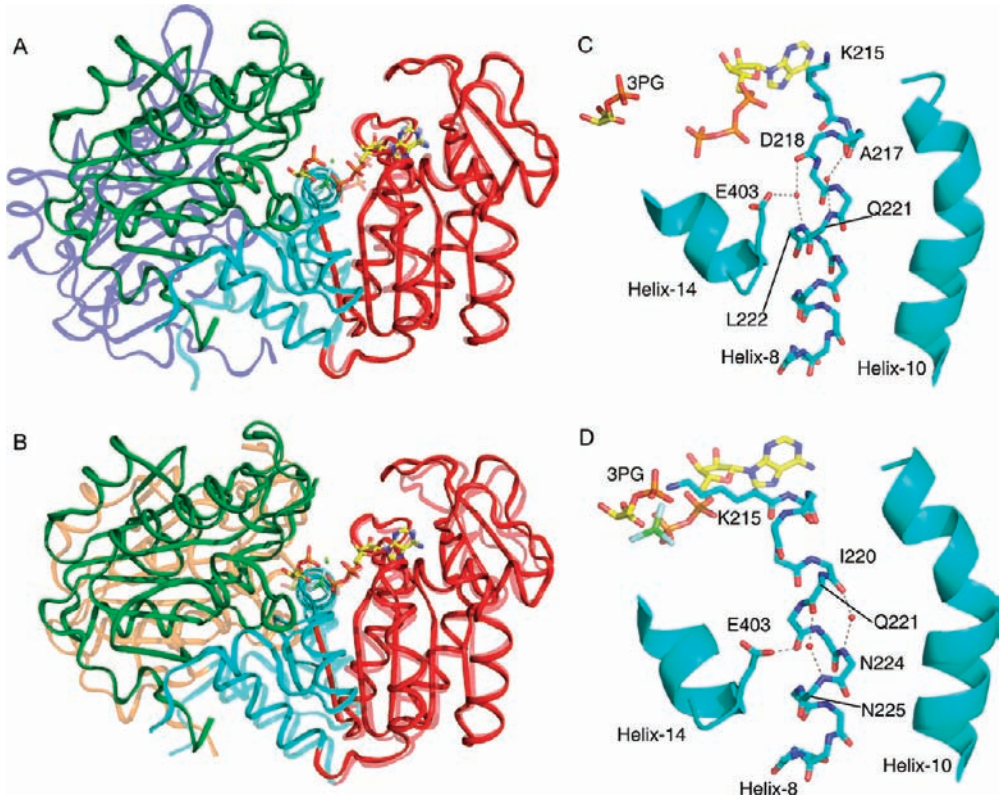

Figure 4. Domain reorientation in the HsPGK-3PG-MgF_3^--ADP TSA complex. (A) HsPGK-3PG-MgF_3^--ADP TSA complex is shown superimposed on the SsPGK-ATP complex (1vjd[28] transparent, including a modeled 3PG ligand), optimized for the C-domain. The ribbon representations are colored so that the C-domain and interdomain region are red and cyan, respectively, in both structures, and the N-domains are colored blue (SsPGK-ATP) and green (HsPGK-3PG-MgF_3^--ADP). The TSA ligands are shown as sticks and catalytic Mg^{2+} as a green sphere. (B) HsPGK-3PG-MgF_3^--ADP TSA complex is shown superimposed on the TbPGK-3PG-ADP complex (transparent), optimized for the C-domain. The ribbon representations are colored as in (A), except that the N-domain of TbPGK-3PG-ADP is colored orange. (C) Two water molecules (red spheres) interrupt the regular hydrogen bonding of helix-8 in the open state of PGK. The positions of these water molecules are preserved between the highest resolution crystal structures of PGK (<2 Å, 2ie8, 1v6s, 1php, 1vjd, 1hdi, 3c3b, 3c39), with the rms deviations of their positions between these structures being 0.32 and 0.45 Å, which are comparable to the equivalent rms deviation for the main-chain of helix-8 (0.39 Å). The relationship of these water molecules to E403 and helix-14 is shown for the SsPGK-ATP complex (1vjd[28]). The relative positions of the side chain of K215 and the (modeled) 3PG ligand in this structure are also indicated. (D) γ-Carboxylate of E403 changes position upon domain reorientation so that, in the HsPGK-3PG-MgF_3^--ADP TSA complex, the two water molecules observed in the open complexes are no longer present. The new position of E403 introduces water molecules into the hydrogen bonds in the second turn of helix-8, changing the bend of the helix so that the side chain of K215 is orientated toward the N-domain and the 3-phosphate of 3PG. The remainder of the C-domain (e.g., helix-10) is relatively unperturbed by domain reorientation.

coordination of the ε-amino group of K215 between the 3-phosphate group of 3PG and the MgF_3^- moiety (see Figure 3A,B).

HsPGK-3PG-AlF_4^--ADP TSA Complex. The identification of three cationic side chains (R38, K215, and K219) that coordinate the MgF_3^- moiety in the HsPGK-3PG-MgF_3^--ADP TSA complex provides an opportunity to test the charge-balance hypothesis. According to the hypothesis, removal of the positive charge associated with one of these side chains should induce a compensatory reduction in negative charge in the metal fluoride moiety. Fluoroaluminate complexes were chosen for this test because AlF_4^- and AlF_3^0 species are populated almost equally in solution under the conditions used here.[39]

Four new ^{19}F resonances result from the addition of $AlCl_3$ to a HsPGK-3PG-MgF_3^--ADP TSA complex (Figure 1B and Table S1, Supporting Information), characteristic of the formation of an AlF_4^- TSA complex.[15] In common with the HsPGK-3PG-MgF_3^--ADP TSA complex, the presence of four well-resolved peaks indicates that each of the fluorine atoms is bound in a distinct site and does not exchange environments on the NMR time scale. Crystals of the HsPGK-3PG-AlF_4^--ADP TSA complex diffracted X-rays to a resolution of 1.5 Å, and the structure was solved by molecular replacement (see Table 1 for data collection and refinement statistics). The structures of the two complexes are almost identical—overall root mean squared (rms) deviation is 0.21 Å for all main-chain heavy atoms, which improves to 0.12 Å at the domain level (Table S3, Supporting Information). The latter improvement arises from the domain orientations of the two complexes differing slightly, the HsPGK-3PG-AlF_4^--ADP TSA complex being closed by a further 0.5°. This coincides with shorter axial coordination distances in the HsPGK-3PG-AlF_4^--ADP TSA complex, bringing the 3PG and ADP groups to within 3.9 Å. The positions of the central metal atoms in the two TSA complexes are within the resolution of the structures (Figure 5).

The square planar geometry of the AlF_4^- moiety has little effect on the active site. Figure 5 shows that, while the geometries of the MgF_3^- and the AlF_4^- moieties are different, the residues responsible for binding the F_1, F_2, and F_3 atoms are identical. Fluorine F_1, coordinated by the catalytic magnesium and K215:Nζ, is located in the same position as F_1 in the HsPGK-3PG-MgF_3^--ADP TSA complex (positional difference = 0.02 Å). The accommodation of F_4 results in a small perturbation of the backbone geometry involving residues

(39) Martin, R. B. *Coord. Chem. Rev.* **1996**, *149*, 23–32.

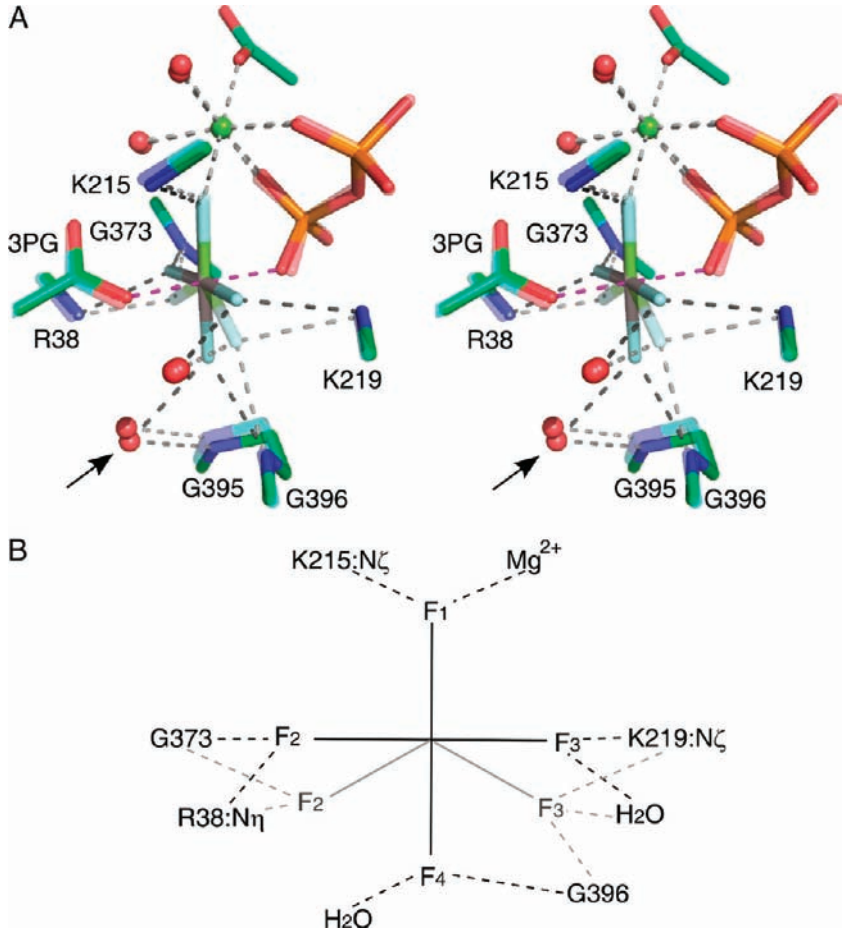

Figure 5. Differences in the coordination of the AlF_4^- and the MgF_3^- moieties between the HsPGK-3PG-AlF_4^--ADP TSA and the HsPGK-3PG-MgF_3^--ADP TSA complexes. (A) Stereo view overlay of the active site regions of the HsPGK-3PG-AlF_4^--ADP TSA (green) and the HsPGK-3PG-MgF_3^--ADP (cyan, transparent) TSA complexes is shown optimized on the metal fluoride coordinating groups (with associated water molecules (red spheres) and catalytic Mg^{2+} (green sphere)). The differences between the two complexes are small, and the same groups coordinate the AlF_4^- moiety (pale blue and gray) as the MgF_3^- moiety (pale blue and green) except for the newly involved water molecule indicated by the arrow (coordinating F_4). The axial O−metal−O bonds are shown as purple dashes, and hydrogen bonds to the fluorine atoms are shown in dark gray (HsPGK-3PG-AlF_4^--ADP) and light gray (HsPGK-3PG-MgF_3^--ADP) dashes. (B) Schematic representation indicating the equivalence of the fluorine atoms between the HsPGK-3PG-AlF_4^--ADP (black) and the HsPGK-3PG-MgF_3^--ADP (gray) TSA complexes.

T393−G396, giving an associated main-chain heavy atom rms deviation of 0.15 Å. Overall, the active site is robust and insensitive to the steric demands of switching from a TBP to an octahedral metal fluoride TSA complex. In particular, the side chain of K219 is in the same position in the two structures.

AlF_3-TSA Complex of Mutant PGK. The single-point mutants K215A and K219A of HsPGK were chosen to test the local charge-balance hypothesis because both have reduced catalytic activity by over 1000-fold without detectable conformational or stability changes for the unliganded protein.[25,31] ^{19}F NMR measurements (not shown) revealed that HsPGK(K215A) did not measurably populate either a magnesium or aluminum fluoride TSA complex. Although small-angle X-ray scattering (SAXS) data are consistent with HsPGK(K215A) being able to form a closed conformation in the presence of ATP and 3PG,[25] diagnostic resonances in the ^1H NMR spectra associated with TSA complex formation (Figure S1, Supporting Information) were absent. In contrast, HsPGK(K219A) formed a fluoroaluminate (but not a fluoromagnesate) complex with 3PG and ADP, resulting in three ^{19}F resonances with a 1:1:1 ratio of integrals (Figure 1C and Table S1, Supporting Information) characteristic of a trifluoroaluminate, AlF_3^0, TSA species. Corresponding changes in the ^1H NMR spectra indicate that the HsPGK(K219A)-3PG-AlF_3^0-ADP TSA complex adopts a closed conformation analogous to the wild-type HsPGK TSA complexes (Figure S1B, Supporting Information). Moreover, HsPGK(K219A) does not measurably bind an AlF_4^- species even at elevated fluoride concentrations (up to 70 mM). Together, these data establish that removal of the positive charge contributed by K219 in the coordination of the TSA in the wild-type system induces a corresponding unit reduction in negative charge through the loss of one fluoride from the aluminum fluoride moiety in the mutant complex. Thus, the chemical mutation arises as a consequence of the protein mutation, and the dominance of AlF_3^0 over AlF_4^- in the HsPGK(K219A)-3PG-AlF_3^0-ADP TSA complex is exactly that predicted by the charge-balance hypothesis.

The HsPGK(K219A)-3PG-AlF_3^0-ADP TSA complex was crystallized under the same conditions as the wild-type HsPGK complexes, and the structure was solved to a resolution of 1.56 Å by molecular replacement (see Table 1 for data collection and refinement details). The differences within the protein between the mutant and wild-type AlF_4^- complexes are minor (overall main-chain heavy atom rms deviation of 0.10 Å). The positions previously occupied by the side chain of K219, including the ε-amino group, are occupied by water molecules

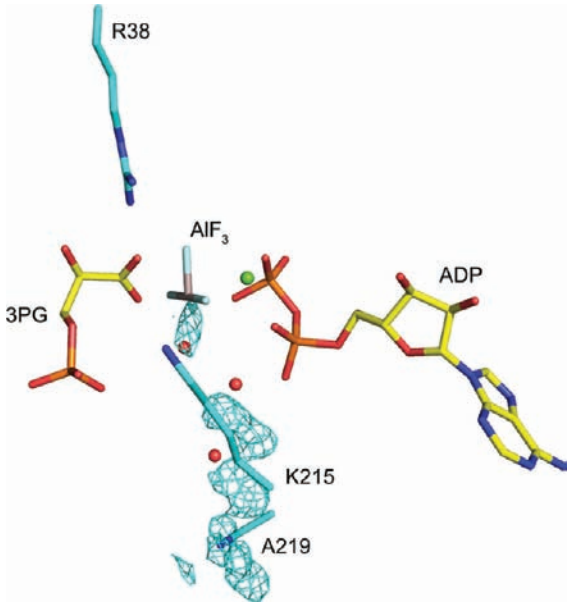

Figure 6. The AlF_3^0 moiety in the HsPGK(K219A)-3PG-AlF_3^0-ADP TSA complex is octahedral. The F_o-F_o electron density difference Fourier map between the HsPGK-3PG-AlF_4^--ADP TSA and the HsPGK(K219A)-3PG-AlF_3^0-ADP complexes is shown as a cyan mesh contoured at 2σ, with the 3PG and ADP ligands and the side chains coordinating the AlF_3^0 moiety in the HsPGK(K219A)-3PG-AlF_3^0-ADP active site shown as sticks. The water and Mg^{2+} are shown as red and green spheres, respectively. A stereo version of this image is available in Supporting Information.

(Figure 6). There is a small perturbation of the residues at the N-terminus of helix-8 (V216−I220: main-chain rms deviation 0.29 Å), most likely linked to the absence of the interaction between K219:Nζ and the AlF_3^0 moiety, allowing a more relaxed conformation in this segment of the helix. However, the hydrogen bonding within helix-8 and its relationship with helix-14 are unaffected by the mutation.

A surprising result from the HsPGK(K219A)-3PG-AlF_3^0-ADP TSA structure is that, unlike all other phosphoryl transfer enzyme TSA complexes previously reported to contain an AlF_3^0 moiety, the aluminum ion has octahedral rather than the TBP geometry. Three of the four equatorial coordinating atoms of the AlF_3^0 moiety can be readily identified as corresponding to F_1, F_2, and F_4 in the HsPGK-3PG-AlF_4^--ADP TSA complex by the coordination distances (1.78 Å, characteristic of Al−F bond lengths), consistent with the three resonances present in the ^{19}F NMR spectrum (Figure 1C). The fourth atom can be assigned as oxygen because of its longer coordinating distance to the aluminum (1.92 Å). This change in Al−X coordination distance results in residual electron density being present in the F_o-F_o Fourier difference map between the data for the HsPGK(K219A)-3PG-AlF_3^0-ADP and the HsPGK-3PG-AlF_4^--ADP TSA complexes (Figure 6). The protonation state of the oxygen atom is readily resolved from the ^{19}F chemical shifts. The observed ^{19}F resonances of the HsPGK(K219A)-3PG-AlF_3^0-ADP TSA complex are significantly downfield from those of the HsPGK-3PG-AlF_4^--ADP TSA complex (Table S1, Supporting Information and Figure 1B,C). This indicates a loss of electron density from the AlF_3^0 moiety, which is consistent with the replacement of F^- by a less electronegative species. Hence, the octahedral aluminum fluoride moiety is assigned as $AlF_3^0 \cdot OH_2$ axially coordinated by ADP and 3PG oxyanion ligands. The fact that a trigonal entity does not form, even in circumstances where an AlF_3^0 moiety is the overwhelmingly preferred metal fluoride, supports the proposal that many previously reported AlF_3^0 TSA complexes of phosphoryl transfer enzymes may, in reality, be MgF_3^- complexes.[15]

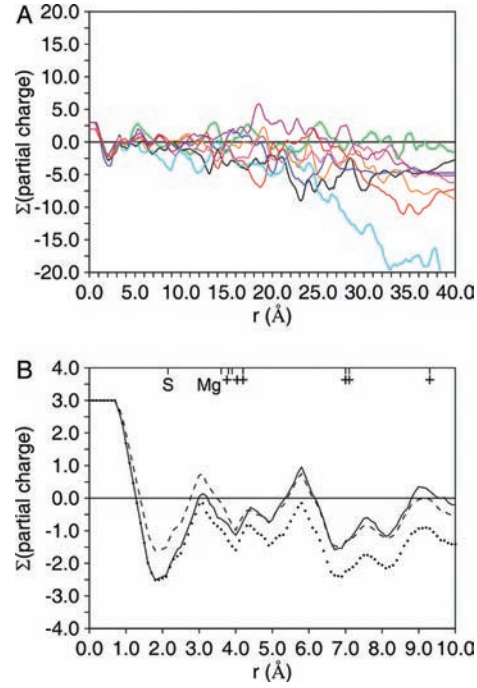

Figure 7. Charge balance across phosphoryl transfer enzyme active sites. (A) Charge balance (expressed as the sum of partial charges) is shown as a function of the radius from the central metal ion of the metal fluoride species in the TSA complexes of HsPGK, and seven nucleotide kinases and hydrolases selected in a previous review of aluminum fluoride TSA complexes.[40] The data are colored as follows (with PDB codes in parentheses): black, HsPGK; blue, UMP kinase (5ukd); green, NDP kinase (1kdn); red, H-Ras:GAP complex (1wq1); cyan, nitrogenase (1n2c); magenta, CDC42:GAP complex (1grn); orange, Rho:GAP complex (1tx4); and purple, G protein α subunit (1gfi). (B) Relationship between the sum of partial charges and radius is shown for the HsPGK-3PG-AlF_4^--ADP TSA complex (solid line), the HsPGK(K219A)-3PG-AlF_3^0-ADP TSA complex (dashed line), and a modeled HsPGK(K219A)-3PG-AlF_4^--ADP complex (dots). The positions of the substrate oxygen atoms (S), the catalytic magnesium (Mg), and the six positively charged residues highlighted in the text (+) are indicated on the top *x*-axis. The balance of charges is significantly more negative over the active site region for the modeled complex.

Charge Balance as a Prevalent Feature of Phosphoryl Transfer. The behavior of HsPGK in the three metal fluoride complexes provides experimental support for the charge-balance hypothesis described above. Analysis of the charge distributions within TSA complexes of several other phosphoryl transfer enzymes shows that local zero net charge is a common feature. The charge distribution across these enzymes was calculated by summing the partial charges within a sphere of defined radius whose origin is the surrogate of the transferring phosphorus atom. Choosing as examples seven phosphoryl transfer enzymes selected in a previous study of the behavior of metal fluoride TSA complexes,[40] we found a common pattern between the net charge and sphere radius (Figure 7A). Within a radius of approximately 4.0 Å, which includes the heavy nuclei involved in only the first layer of hydrogen bonding, the metal fluoride charge is compensated by charges in the active site and the net charge is zero. This charge balance is maintained out to at least 6.0 Å and further in some proteins. (These calculations were made using the interpretation that all of the TBP-coordinated,

(40) Schlichting, I.; Reinstein, J. *Nat. Struct. Biol.* **1999**, *6*, 721–723.

trifluoro-metal species are MgF_3^- species. Calculations with vanadate and nitrate TSA complexes show the same pattern.) Similarly, in HsPGK TSA complexes, the charges from seven cationic groups of the enzyme (R38, R65, R122, and R170 from the N-domain and K215, K219, and D374-Mg^+ from the C-domain) balance the charges from the seven anionic groups of the TSA ligands (3 on ADP, 3 on 3PG and 1 on MgF_3^- or AlF_4^-). By contrast, modeling of the putative HsPGK(K219A)-3PG-AlF_4^--ADP complex and a repeat of the calculation results in a net charge close to −1 at a radius of 6.0 Å (Figure 7B).

Experimental evidence for the importance of electrostatic interactions in biological catalysis has been reported for enzymes as diverse as chorismate mutase,[41] subtilisin,[42] and uracil−DNA glycosylase[43] and has much support from computational studies.[44,45] However, in the case of phosphoryl transfer enzymes, it is the balance of charges that appears to be particularly important, where the attack on a dianionic phosphate group by a negatively polarized nucleophile is extremely unfavorable because of Coulombic repulsion.[9,46] The inference is that enzymes have evolved to counteract the repulsion through fine-tuning the active site to the charge of the TS. This property of phosphoryl transfer enzymes has implications for a number of previously reported phenomena involving members of this family. For example, in a mutagenesis study of phosphofructo-1-kinase,[47] the loss of activity associated with removal of an aspartate residue (D127S) is partially reversed by a second mutation, R252Q, that would restore the balance of charge in the active site. In a more general context, arginine finger residues that regulate phosphoryl transfer complete charge balance within the active complex in an analogous manner to that seen for K219 in the HsPGK active site. Examples of this include the activation of G-proteins by G-protein activating proteins (GAPs),[48−50] the Aha1 activation of Hsp90[51] and the subunit−subunit interactions of F_1-ATPase,[52] AAA+ ATPases,[53] and DNA helicases.[54] In these systems, the arginine finger is contributed from a protein chain other than that creating the rest of the active site. The rate enhancement achieved by the presence of the arginine side chain in the active site is ca. 2000-fold in the Ras−RasGAP complex,[50] similar to that seen for the contribution of K219 in HsPGK (ca. 1000-fold[25]).

Conclusions

The structures of the MgF_3^- and AlF_4^- TSA complexes of HsPGK provide the first experimental description of the fully closed state of PGK. The power of ^{19}F NMR to report on the local electrostatic and protonic environments of metal fluoride TSAs has been used to assign the electron density resulting from X-ray diffraction data by resolving the nature of the various metal fluoride TSA complexes populated. The dominance of MgF_3^- and AlF_4^- TSA species in the active site of wild-type HsPGK and the inhibition of PGK at elevated concentrations of nitrate,[55] another trigonal monoanion, support the hypothesis that zero local net charge is a key feature of phosphoryl transfer enzyme transition states. The switch in the metal fluoride moiety in the active site from AlF_4^- to AlF_3^0 in the K219A mutant complex of HsPGK demonstrates experimentally that the environment surrounding the transferring phosphate group in near-TS conformations is strongly predisposed toward charge balance. The dominance of charge balance in TSA binding can guide the design of drugs targeted to or activated by phosphoryl transfer enzymes (such as L-nucleoside analogues), whether these are TSA-based pharmaceuticals[56] or compounds that target the active sites of the catalytically inactive forms of proteins (such as G-proteins without GAPs).

Experimental Procedures

Source of Proteins. Expression and purification of recombinant wild-type HsPGK as well as its K215A and K219A mutants were described earlier.[25,31]

NMR. NMR samples were typically composed of 0.2 mM HsPGK in 50 mM Tris (pH 7.5), 3 mM NaN_3, 50 mM DTT, and 10% v/v D_2O. Increased concentrations of reducing agent relative to those used previously for GsPGK prevented intermolecular disulfide bridge formation. The HsPGK-3PG-MgF_3^--ADP TSA complex was generated by the addition of 5 mM ADP, 10 mM 3PG, 5 mM $MgCl_2$, and 10 mM NH_4F. Subsequently, the HsPGK-3PG-AlF_4^--ADP TSA complex was prepared by the addition of 2 mM $AlCl_3$ to the sample defined above. Spectra were recorded at 298 K on a Bruker Avance 500 MHz spectrometer equipped with a 5 mm dual $^1H/^{19}F$ probe.

Crystallization. Lyophilized HsPGK was resuspended in 50 mM Tris (pH 7.5), 20 mM DTT, 25 mM $MgCl_2$, 50 mM 3PG, and 10 mM ADP. The HsPGK-3PG-MgF_3^--ADP TSA complex was supplemented with 20 mM NH_4F and 1 mM deferoxamine, which was included to chelate any contaminating aluminum. The HsPGK-3PG-AlF_4^--ADP TSA complex samples were supplemented with 20 mM NH_4F and 5 mM $AlCl_3$. The final protein concentration was 15 mg mL^{-1}. Previously determined conditions[57] produced crystals in the open form of the protein, but no density for either metallofluoride was observed in the difference Fourier maps. New crystallization conditions were screened for at the High Throughput Crystallization Laboratory,[58] the Partnership for Structural Biology (PSB), Grenoble, France. Crystals with the approximate dimensions of 0.5 × 0.1 × 0.05 mm were obtained by vapor diffusion in 4 μL sitting drops of 50:50 mix of protein solution and precipitant (28−33% PEG 2000 MME and 0.1 M Bis/Tris pH 6.5). Prior to harvesting, the PEG 2000 MME concentration was increased to

(41) Kienhofer, A.; Kast., P.; Hilvert, D. *J. Am. Chem. Soc.* **2003**, *125*, 3206–3207.
(42) Jackson, S. E.; Fersht, A. R. *Biochemistry* **1993**, *32*, 13909–13916.
(43) Jiang, Y. L.; Ichikawa, Y.; Song, F.; Stivers, J. T. *Biochemistry* **2003**, *42*, 1922–1929.
(44) Warshel, A.; Sharma, P. K.; Kato, M.; Xiang, Y.; Liu, H. B.; Olsson, M. H. M. *Chem. Rev.* **2006**, *106*, 3210–3235.
(45) Dinner, A. R.; Blackburn, G. M.; Karplus, M. *Nature* **2001**, *413*, 752–755.
(46) Westheimer, F. H. *Science* **1981**, *235*, 1173–1178.
(47) Zheng, R.-L.; Kemp, R. G. *Biochem. Biophys. Res. Commun.* **1995**, *214*, 765–770.
(48) Scheffzek, K.; Ahmadian, M. R.; Kabsch, W.; Wiesmuller, L.; Lautwein, A.; Schmitz, F.; Wittinghofer, A. *Science* **1997**, *277*, 333–338.
(49) Rittinger, K.; Walker, P. A.; Eccleston, J. F.; Smerdon, S. J.; Gamblin, S. J. *Nature* **1997**, *389*, 758–762.
(50) Ahmadian, M. R.; Stege, P.; Scheffzek, K.; Wittinghofer, A. *Nat. Struct. Biol.* **1997**, *4*, 686–689.
(51) Meyer, P.; Prodromou, C.; Liao, C.; Hu, B.; Roe, S. M.; Vaughan, C. K.; Vlasic, I.; Panaretou, B.; Piper, P. W.; Pearl, L. H. *EMBO J.* **2004**, *23*, 511–519.
(52) Bowler, M. W.; Montgomery, M. G.; Leslie, A. G. W.; Walker, J. E. *J. Biol. Chem.* **2007**, *282*, 14238–14242.
(53) Putnam, C. D.; Clancy, S. B.; Tsuruta, H.; Gonzalez, S.; Wetmur, J. G.; Tainer, J. A. *J. Mol. Biol.* **2001**, *311*, 297–310.
(54) Niedenzu, T.; Roleke, D.; Bains, G.; Scherzinger, E.; Saenger, W. *J. Mol. Biol.* **2000**, *306*, 479–487.
(55) Scopes, R. K. *Eur. J. Biochem.* **1978**, *85*, 503–516.
(56) Schramm, V. L. *J. Biol. Chem.* **2007**, *282*, 28297–28300.
(57) Gondeau, C.; Chaloin, L.; Lallemand, P.; Roy, B.; Perigaud, C.; Barman, T.; Varga, A.; Vas, M.; Lionne, C.; Arold, S. T. *Nucleic Acids Res.* **2008**, *36*, 3620–3629.
(58) Dimasi, N.; Flot, D.; Dupeux, F.; Marquez, J. A. *Acta Crystallogr. F* **2007**, *63*, 204–208.

35% for cryoprotection. Crystals were harvested with a micromount (MiteGen, Ithica, NY), plunged into liquid nitrogen and stored at 100 K.

Data Collection and Refinement. Diffraction data were collected from cryo-cooled crystals to a maximum of 1.47 Å resolution (see Table 1) on an ADSC Q210 CCD detector at beamline ID14-2 at the European Synchrotron Radiation Facility (ESRF), Grenoble, France. No satisfactory molecular replacement solution was found using the available structures of HsPGK, so separate solutions were found for the two domains using residues 1−190 and 191−416 from HsPGK (PDB accession code 3c39) and then combined. A 90% complete model for the HsPGK-3PG-MgF_3^--ADP TSA complex was then built by Arp/Warp[59,60] using the phases from the combined molecular replacement solutions. Ligands were not included until the final rounds of refinement so that they could be built into unbiased difference Fourier maps. Subsequent structures used the HsPGK-3PG-MgF_3^--ADP TSA complex as a search model with bound ligands and water molecules removed.

Charge-Balance Calculations. Partial charges from the standard CNS-Xplor[61] parameter files for proteins were used. Each heavy atom was treated as a sphere with a radius of 1.0 Å, with the integral charge across the sphere equaling the partial charge. The contribution from each heavy atom was then divided among 0.1 Å "bins" according to their distance from the central ion of the metal fluoride moiety, and the partial charge within each bin was summed.

Data Deposition. The atomic coordinates and structure factors have been deposited in the protein data bank with the following codes: HsPGK-3PG-MgF_3^--ADP (2wzb), HsPGK-3PG-AlF_4^--ADP (2wzc), and HsPGK(K219A)-3PG-AlF_3^0-ADP (2wzd).

Acknowledgment. This research was supported by the Biotechnology and Biological Sciences Research Council UK as well as by the grants OTKA (NK 77978) of the Hungarian National Research Fund. M.V., A.V., and J.S. are very thankful to Prof. P. Závodszky, director of Institute of Enzymology, Hungarian Academy of Sciences, for his interest in the work.

Supporting Information Available: Data processing methods; 1D ^1H NMR spectra; schematic of catalytic Mg^{2+} coordination; stereo views of electron density difference maps; tables of fluorine NMR spectral parameters, dihedral angles, and rms deviations between PGK structures. This material is available free of charge via the Internet at http://pubs.acs.org.

JA100974T

(59) Cohen, S. X.; Morris, R. J.; Fernandez, F. J.; Ben Jelloul, M.; Kakaris, M.; Parthasarathy, V.; Lamzin, V. S.; Kleywegt, G. J.; Perrakis, A. *Acta Crystallogr. D* **2004**, *60*, 2222–2229.
(60) Cohen, S. X.; Ben Jelloul, M.; Long, F.; Vagin, A.; Knipscheer, P.; Lebbink, J.; Sixma, T. K.; Lamzin, V. S.; Murshudov, G. N.; Perrakis, A. *Acta Crystallogr. D* **2008**, *64*, 49–60.
(61) Brunger, A. T. *Nat. Protoc.* **2007**, *2*, 2728–2733.